Antibacterial Action and Target Mechanisms of Zinc Oxide Nanoparticles Against Bacterial Pathogens

Carolina Rosai Mendes (carolina.rosai@unesp.br)
Sao Paulo State University (UNESP)
Guilherme Dilarri
Sao Paulo State University (UNESP)
Carolina Froes Forsan
Sao Paulo State University (UNESP)
Vinícius de Moraes Ruy Sapata
Sao Paulo State University (UNESP)
Paulo Renato Matos Lopes
Sao Paulo State University (UNESP)
Peterson Bueno de Moraes
State University of Campinas (UNICAMP)
Renato Nallin Montagnolli
Federal University of Sao Carlos (UFSCar)
Henrique Ferreira
Sao Paulo State University (UNESP)
Ederio Dino Bidoia
Sao Paulo State University (UNESP)

Research Article

Keywords: Nanomaterial, Metal oxide, Bactericidal mechanism of action, Membrane integrity, Interference on the FtsZ ring.

Posted Date: November 12th, 2021

DOI: https://doi.org/10.21203/rs.3.rs-1054432/v1

Version of Record: A version of this preprint was published at Scientific Reports on February 16th, 2022. See the published version at https://doi.org/10.1038/s41598-022-06657-y.

Abstract

Zinc oxide nanoparticles (ZnO NPs) are one of the most widely used nanoparticulate materials due to their antimicrobial properties, but their main mechanism of action (MOA) has not been fully elucidated. The study characterized ZnO NPs using X-ray diffraction, FT-IR spectroscopy and scanning electron microscopy. Antimicrobial activity of clinically bacteria *Escherichia coli*, *Staphylococcus aureus*, *Bacillus subtilis* and *Pseudomonas aeruginosa* was evaluated by REMA after exposure to the ZnO NP at concentrations from 0.2 to 1.4 mM. Sensitivity was achieved at 0.6 mM for the Gram-negatives and 1.0 mM for Gram-positives cells. The effect of ZnO NPs on the membrane integrity and in the interference of cell division was investigated by its effect on the divisional ring, through fluorescence microscopy assays using *B. subtilis* (amy::pspac-ftsZ-gfpmut1) expressing FtsZ-GFP. Results showed that ZnO NPs did not interfere with the assembly of the divisional Z-ring. However, 70% of the cells showed damage in the cytoplasmic membrane after 15 min of exposure to the ZnO NPs. Electrostatic forces, production of Zn^{2+} ions, generation of reactive oxygen species were described as pathways of bactericidal action by ZnO. Thus, understanding bactericidal MOA can produce predictive models to prevent bacterial resistance and lead to further research.

Introduction

Nanoparticles (NPs) of metal oxide were highlighted in the field of antimicrobial compounds by catalytic inhibition [1-2]. However, the bactericidal mechanism of action (MOA) is dependent on several parameters such as morphology, composition and concentration of the NPs [3]. Zinc oxide (ZnO), magnesium oxide (MgO), titanium dioxide (TiO_2) are substances recognized as safe when used in food additives or drug delivery according to the Food and Drug Administration (FDA 2011) US Code of Federal Regulations (Title 21-CFR 182.8991) [4]. Zinc oxide nanoparticles (ZnO NPs) is the most promising inorganic material that has bactericidal action and is found in the composition of pharmaceutical drugs, sanitizers, cosmetics and food packaging processes [5]. However, the target of MOA in clinical bacteria is not fully studied. Zanet et al. [6] carried out experiments using ZnO NPs against model cell of *Saccharomyces cerevisiae* in order to elucidate the main MOA, and conclude that ZnO NPs effect depends on their own composition and dose.

The synthesis of ZnO NPs can be achieved by chemical precipitation [7]; salt reduction [8]; sol-gel way based on an acetate precursor [9] and sonochemical synthesis [10]. However, each synthesis produces a ZnO particle of variable morphology and size [11-8-12]. Thus, the MOA, as well as its interaction with cell structures, can be varied and diverse.

ZnO is a transition metal oxide and semiconductor with high binding energy which allows for a highly oxidative character [13]. This reaction leads to the formation of reactive oxygen species as the pathways of bactericidal action. In addition, another bactericidal MOA occurs through the releasing of zinc ions, which (Zn^{2+}), which damage the cell membrane and can interrupt some metabolic pathways [14]. Thus, more studies about the antibacterial MOA of ZnO NPs, can provide important contributions to predict possible mechanisms of bacterial resistance and optimize contact time for effective inhibition. Cell division is a critical process for microbial survival. Among the proteins involved in this process, FtsZ has a pivotal function in which it serves as a scaffold for the assembly of a multiprotein complex structure, the divisome, responsible for coordinating all the steps of cell division and cell wall remodeling [15]. The protein acts during cell division as an organizer of the cytoplasmic ring in bacteria and can be considered the main target of several bactericidal compounds [16]. Bactericidal agents act in diverse ways, such as inhibition of FtsZ in the cell division pathway, and can be identified by cytological profile with cells expressing FtsZ-GFP, as observed by fluorescence microscopy [17].

In this study, a set of clinically relevant bacteria *Escherichia coli* (ATCC 8739), *Staphylococcus aureus* (ATCC 6538), *Bacillus subtilis* (ATCC 19659) and *Pseudomonas aeruginosa* (ATCC 27853) were used to evaluate the effect on the cytological profile and determine the inhibitory concentration of ZnO NPs. The authors focused the study on the evaluation of the ZnO NPs action on the cell morphology, DNA damage, and protein production; therefore, the cytoplasmatic membrane and other proteins, such as FtsZ, which forms the scaffold for the divisome, were not included in the spectra of

analysis. FtsZ in *Bacillus subtilis* cell culture was used to evaluate any interference in the formation of the FtsZ ring in the divisional septum. It is important to clearly elucidate the MOA of any kind of antimicrobial compound in order to avoid bacterial resistance.

Material And Method

Synthesis of ZnO NPs

All reagents were purchased from Sigma-Aldrich (Taufkirchen, Germany). ZnO NPs was synthesized by sonochemical-coprecipitation of 2 mM solution of zinc chloride followed by dripping it with ammonium hydroxide [18]. Next, the mixture was heated to 60°C under continuous stirring until complete precipitation. The precipitate underwent ultrasonic bath sonicator (USC 1400) for 30 minutes to obtain NPs, followed by vacuum filtration in a 0.22 µm cellulose membrane, washing with deionised water and finally drying at 100°C overnight.

Characterization of the synthesized nanomaterial

ZnO NPs were characterized using Fourier transform infrared spectrophotometer FT-IR (Shimadzu Model 8300), adjusted for scanning at 4000-400 cm^{-1}. For the analysis, a KBr pellet was made with the nanomaterial sample [19]. Micrographs of ZnO NPs were taken by Scanning Electron Microscope (SEM) - JEOL JSM-IT100 operated at 30 kV coupled to a Bruker Quantax Energy Dispersive Detector (EDS), in order to study the morphological characteristics. The samples were coated by a gold layer by metalization process before SEM readings. Finally, the crystalline structure of the ZnO NPs was characterized by X-ray diffraction powder (XRD, PHILIPS, X' pert-MPD system) using Cu Kα radiation (λ = 1.5418 Å). The X-ray wavelength was 0.15418 nm and the diffraction patterns were measured in the range of 2θ from 20° to 65°.

Bacterial strain and growth conditions

Escherichia coli (ATCC 8739), *Staphylococcus aureus* (ATCC 6538), *Bacillus subtilis* (ATCC 19659), *Pseudomonas aeruginosa* (ATCC 27853) and the mutant *Bacillus subtilis* (*amy*::*pspac-ftsZ-gfpmut1*) expressing FtsZ-GFP were cultivated in nutrient broth medium (5 g L^{-1} of peptone; 3 g L^{-1} of beef extract; for solid medium was added 15 g L^{-1} of bacterial agar) at 28°C for 24 hours in shaker at 200 rpm. All reagents for cellular growth were purchased from Himedia Laboratories Ltd. (Mumbai, India).

Antibacterial activity assay

E. coli, *S. aureus*, *B. subtilis* and *P. aeruginosa* were used to measure sensitivity after ZnO NP exposure. Antibacterial activity was determined by the Resazurin Microtiter Assay (REMA) to determine inhibitory concentrations (ICs) of ZnO NPs [20]. ZnO NPs at concentrations between 0.2 to 1.4 mM were placed in 96-well microplates. The strains were inoculated to independent trials at a final concentration of 10^5 cells per 100 µL in each well and incubated for 12 hours at 30 ± 1°C.

Nisin at 5 $\mu g.mL^{-1}$ and Kanamycin at 20 $\mu g.mL^{-1}$ from Sigma-Aldrich (Taufkirchen, Germany) were used for the reference antibiotic in positive controls to Gram-positive and Gram-negative bacteria, respectively. Nutrient broth medium was used for the negative control. After the incubation period, the inhibition of cell growth was measured by the addition 0.1 $mg.mL^{-1}$ of resazurin from Sigma-Aldrich (Taufkirchen, Germany) in each well. Resazurin is a redox indicator prone to NAD^+ reduction to resorufin (a fluorescent red-colour compound) when there is cell activity [17]. The fluorescence intensity of resorufin was detected in a plate reader (Synergy® H1N1 - BioTek, Winooski, VT, USA) set to excitation and emission wavelengths of 530 and 590 nm, respectively. The results of this assay were used to plot the correlation between ZnO NPs concentration and the inhibition of cell growth; and to determine the percentage of IC_{100} (100% inhibitory concentration).

Effect of ZnO NPs on the membrane integrity

E. coli, *P. aeruginosa*, *B. subtilis* and *S. aureus* at 10^5 cells were exposed to ZnO NPs with concentration equivalent to IC_{100} in 100 µL of volume for 15 min per treatment. Next, 900 µL of phosphate buffer was added to stop the reaction. Then, it was added PI (propidium iodide) at 0.01 $mg.mL^{-1}$ and DAPI (4',6-diamidino-2-phenylin-dole) at 0.02 $mg.mL^{-1}$ for each analysis. DAPI stains the nucleoid of every cell, whereas propidium iodide (PI) is a nucleic acid dye that penetrates only cells with damage in the cytoplasmatic membranes. Untreated cells were used as negative control, while positive control for damaged membranes was generated by heat-shock stress.

B. subtilis (*amy*::*pspac-ftsZ-gfpmut1*) mutant expressing FtsZ-GFP was used to investigate the potential of the compound to interfere with the division septa. The bacterial cells were cultivated in the presence of 0.02 mM Isopropyl β-D-thiogalactopyranoside (IPTG) to induce the expression of FtsZ-GFP from the *pspac* promoter. Next, 100 µL of the medium containing 10^5 cells were exposed for 15 minutes with ZnO NPs at IC_{100} concentration. Cells were washed in water and resuspended in 100 µL of 0.85% NaCl solution [17].

Cells were immobilized onto agarose-covered slides and subsequently analysed by fluorescence microscopy technique using an Olympus BX-61 (Tokyo, Japan), equipped with a monochromatic camera OrcaFlash 2.8 (Hamamatsu, Japan). Images were processed by the software CellSens version 11 (Olympus). The trial considered 100 individuals (n = 100) per treatment for quantification.

Results And Discussion

Characterization of ZnO NPs

The XRD peaks were consistent as ZnO crystallite. The analysis showed no extra peaks, which is due to the purity of the material applied during the synthesis of ZnO NPs. The positions of the diffraction peaks showed the same pattern found in the Joint Committee on Powder Diffraction Standards: 36-1451 database (JCPDS).

Figure 1 shows the diffraction peaks of ZnO NPs at (100), (002), (101), (102), (110), (103) correspond respectively to the values in degrees (2θ) at 31.34°, 34.50°, 36.32°, 47.60°, 56.68°, 62.94°. High diffraction peaks indicated the crystalline nature of the material [21].

Table 1 shows the values of the structural parameters used to calculate the size of the ZnO crystallite by Equation (1) [22]. The high intensity peaks at (100), (002) and (101) were used to determine the lattice parameters.

$$D = \left[\frac{0.9\lambda}{\beta cos\theta}\right] x100 \quad \text{Equation (1)}$$

Where D is the size of the ZnO crystallite; λ is the wavelength of Cu Kα radiation at 1.5418 Å; θ is the Bragg diffraction angle, and β is the full width at half maximum intensity of the diffraction peak of the sample.

Table 1
Structural parameters of ZnO crystallite.

Lattice parameters a (Å)	Lattice parameters c (Å)	c/a ratio	Volume of unit cell (Å^3)	Average crystallite size (nm)	Microstrain ε (×10^3)
3.24	5.21	1.608	47.48	82.38	0.47

The crystallite size can be measured more accurately by high resolution X-ray diffraction (HRXRD) using the Bond method, which increases peak resolution to find the values of the Lattice parameters [22-23]. In this study, we determined by XRD

powder that most synthesized ZnO crystallites are around 80 nm in size. Similar results obtained through the synthesis of ZnO NPs by sonochemical-coprecipitation were shown by Khataee et al. [24].

The surface appearance and morphology of synthesized ZnO NPs were analyzed by SEM at 29.0 kx. Based on the images in Figure 2, the ZnO NP showed complex bead and rod morphology. In addition, the ZnO NPs have an irregular size with formation of aggregated nanocrystallite.

FT-IR spectra are like molecular fingerprints that provide a valuable insight into chemical structures and their changes due to interactions with other molecules [19]. FT-IR analyses detected the characteristic functional group associated with the ZnO NPs, shown in Figure 3. The peak at 575 cm^{-1} corresponds to bond metal-oxygen in Zn–O stretching vibrations. The peak at 3713 cm^{-1} was carbon residues identified during sample measurement; and 1210 cm^{-1} belongs to elongation of C–O. Hydrogen bond is displayed at 1690 and 2346 cm^{-1} is ascribed to the stretching vibration of hydroxyl compounds. The hydroxyl group influences photocatalytic reactions in ZnO by generating superoxide radicals, which act as an antimicrobial [25].

Antimicrobial activity

The bactericidal activity of ZnO NPs against *E. coli*, *P. aeruginosa*, *S. aureus* and *B. subtilis* was evaluated by monitoring the cell respiration. Polynomial regression applied to the dose-response data was used to extrapolate the IC_{100} values, which were expressed as mM. The decrease in cell numbers observed after treatment is shown in Figure 4 by the plot containing the concentration of ZnO NPs versus the inhibition of cell growth.

ZnO NPs showed growth inhibition against *E. coli* and *P. aeruginosa* in IC_{100} values at 0.6 mM for both strains. The IC_{100} values for *B. subtilis* and *S. aureus* were reached at concentrations of 0.8 and 1.0 mM, respectively.

Gram-negative bacteria have a thin layer of peptidoglycan between two membrane lipopolysaccharides and proteins, which provide cellular resistance [26]. In addition, dissociated carboxyl groups present in the cell membrane generate negative charges on the surface. ZnO NPs, on the other hand, have a positive charge, with a zeta potential of +24 mV [27]. As a result of electrostatic forces, damage to the cell membrane occurs due to electrostatic gradient differences across the negative membrane and the positive charges of the Zn^{2+} ions. Therefore, *E. coli* and *P. aeruginosa* cells achieved cell death at the lowest concentration of ZnO NPs. Although the present study did not observe a large difference in the IC values for Gram-negative and Gram-positive, it is noteworthy that Gram-positive exhibited IC_{100} values higher than Gram-negative. Similar inhibition in Gram-negative bacteria was previously reported by Yusof et al. [28], Saqib et al. [29] and Zubair and Akhtar [30]; however, with slight variations in the IC_{100} values due to differences in the synthesis of the nanomaterial, which yields unique characteristics to each one of them. Overall the results were close; however, our study not only investigated the percentage of inhibitory growth, but also the MOA target of ZnO NPs in clinical strains.

Effect of ZnO NPs on the bacteria cell

Bacterial cell division is a complex and dynamic process, which starts by the polymerization of the FtsZ protein in order to assemble the divisome, which will guide all the processes related to cell division and cell wall synthesis and remodelling [31]. FtsZ is the ancestral tubulin conserved in bacteria, which exerts its function dependent on the nucleotide guanosine triphosphate (GTP) [32-33]. Some bactericidal compounds act by preventing the GTPase activity of FtsZ, which will inhibit cell division and lead to cell death [16]. In addition, blockage of the cell division process generally leads to cell filamentation, which can be easily accessed by fluorescence microscopy. Alternatively, by using mutant cells expressing labelled division proteins, e.g. FtsZ-GFP, one can follow the dynamics of division and study the effects compounds might have on the process.

B. subtilis expressing FtsZ-GFP was exposed to ZnO NPs at its IC_{100} for 15 minutes, and after observed under the microscope (Figure 5). Note that even after exposure cells still have intact bars perpendicular to the long axis of the rods, which is the normal profile for the Z-ring. This cytological profile was comparable to the control and did not show any disruption of the divisional ring.

The integrity of the membranes of *E. coli*, *P. aeruginosa*, *S. aureus*, and *B. subtilis* cells was also investigated upon compound exposure using fluorescence microscopy. The results showed the disruption of cytoplasmic membranes in all strains after 15 min of exposure at IC_{100} (Figure 6). The filters Tx Red and DAPI Blue were applied together and used to visualize PI and DAPI. Cells with intact membranes are artificially stained in blue, while cells with damaged membranes are stained red [34]. Thus, an increase in red-stained cells by PI is related to the increase in cell permeability due to damaged membranes.

In this study, all species of bacteria had their cytoplasmic membrane affected within the first 15 minutes of exposure to ZnO NPs. Over 70% cells died with detectable membrane damage. This result shows the ZnO NPs efficacy towards bacterial surface acting at the very initial contact and targeting it's as the first structure nanoparticles comes into contact with. These results were expected as ZnO NPs bactericidal activity was already known, and its predominant MOA is associated with the membrane cell [13]. Because ZnO is a transition metal oxide and semiconductor (which belongs to class II-VI) with wide band gap (3.3 eV), there is a general pattern expected. When the radiation has energy larger than the band gap of the ZnO, electron-hole pairs are formed. Electrons are promoted to the conduction band (CB). The hole generated in the valence band (VB) gets a strongly oxidizing character and oxidizing sites are created, which are capable of oxidizing water molecules or hydroxide anions and generate strong oxidizing species [12]. This reaction leads to the redox chain reaction with the generation of reactive oxygen species (ROS) formed by hydroxyl radical ($^{\bullet}OH$), hydroperoxyde radical ($^{\bullet}HO_2^-$) and superoxide radical anion ($O_2^{\bullet -}$) as the pathways of bactericidal action [35].

Oxidative stress in the bacterial cell can be induced by ROS generation produced from ZnO NPs, which leads to the inhibition of protein synthesis and DNA replication [13]. In this situation, ZnO conductivity increases, close to the "*band gap*" of the UV-spectrum characterized by high emission energy. The electronic excitation can destabilize the charges present in the cytoplasmic membrane resulting in their rupture. ZnO can also damage the cytoplasmic membrane by releasing Zn^{2+} ions from the dissolution of ZnO in aqueous solution. The Zn^{2+} ion acts as an inhibitor of the glycolytic enzyme through the thiol group oxidation due to specific affinity for the sulphur group [3].

The MOA reported in this study are represented in schematic drawing shown in Figure 7.

ZnO NPs are attached in the surfaces of Gram-positive and Gram-negative bacteria through different patways. Teichoic acid in the peptidoglycan layer and lipoteichoic acid in the membrane are the source of negative charges from cell walls. Positive charges from ZnO NPs are attracted to the cell surface by electrostatic interactions, and the difference in electrostatic gradient, which leads to damage in the cell surface [36-37].

Teicoic and lipoteichoic acids act as a chelating agent with Zn^{2+} ions, which is carried by passive diffusion across membrane proteins (Figure 8). Moreover, the bactericidal action can occur by different mechanisms, such as adsorption in the bacterial surface, formation of different intermediates and electrostatic interactions.

The electrochemical gradient is generated by the movement of hydrogen ions across the cell membrane, which facilitates the diffusion of metallic ions [35]. This mechanism is associated with the size of the material, whose small particles would have better electrostatic interactions. Thus, the ZnO target for inhibitory action is dependent on different factors such as concentration, size and time of interaction.

Zanet et al. [6] showed that ZnO NPs affect the cell morphology and DNA. However, this can be a side effect, since the main target of ZnO NPs ends up being the first structure they have contact with and consequently act, such as the cytoplasmic

membrane. Siddiqi et al. [12] through SEM and TEM analysis concluded that ZnO NPs damage the cell membrane, and right after go to the cytoplasm, where they interact with other cell structures. Our results also showed damage to the cell. Therefore, it can be concluded that ZnO NPs are multi-target compounds and affect several structures of bacteria cells, but their main mechanism of action is in the cytoplasmic membrane, being other structure effects a consequence/secondary effect after the membrane rupture.

Declarations

Conflict of Interest Statement

Authors declare that the research was conducted in the absence of any commercial or financial relationships that could be construed as a potential conflict of interest.

Author contributions

C. R. Mendes, G. Dilarri: conceptualization, methodology, fluorescence microscopy analyses, FT-IR assays, validation, formal analysis, writing original draft; C. F. Forsan, V. M. R. Sapata, P. R. M. Lopes, and E. D. Bidoia: methodology, formal analysis; H. Ferreira: conceptualization, methodology, funding acquisition, supervision, writing original draft; P. B. de Moraes: SEM and X-ray assays, writing original draft; R. N. Montagnolli: conceptualization, visualization, writing/review and editing, supervision, funding acquisition, project administration.

Acknowledgements

This study received support from Coordenação de Aperfeiçoamento de Pessoal de Nível Superior (CAPES) - Brazil. Guilherme Dilarri received a PhD scholarship from Fundação de Amparo à Pesquisa do Estado de São Paulo (FAPESP) (process - 2017/07306-9). Henrique Ferreira received grant from FAPESP (process - 2015/50162-2).

References

1. Pachaiappan, R., Rajendran, S., Show, P. L., Manavalan, K. & Naushad, M. Metal oxide nanocomposites for bactericidal effect: a review. *Chemosphere***272**, 128607; https://doi.org/10.1016/j.chemosphere.2020.128607 (2020).
2. Padilla-Cruz, A. L. *et al.* Synthesis and design of ag–fe bimetallic nanoparticles as antimicrobial synergistic combination therapies against clinically relevant pathogens. *Sci.Rep.* **11**, 5351; https://doi.org/10.1038/s41598-021-84768-8 (2021).
3. Qi, K., Cheng, B., Yu, J. & Ho, W. Review on the improvement of the photocatalytic and antibacterial activities of ZnO. *J. Alloys Compounds***727**, 792-820; https://doi.org/10.1016/j.jallcom.2017.08.142 (2017).
4. FDA (2011) Part 182 - Substances generally recognized as safe. Food and drug administration, Washington DC, USA. Available at: http://ecfr.gpoaccess.gov/cgi/t/text/text-idx?c=ecfr&sid=786bafc6f6343634fbf79fcdca7061e1&rgn=div5&view=text&node=21:3.0.1.1.13&idno=21#21:3.0.1.1.13.9. Accessed 21 November 2021.
5. Kołodziejczak-Radzimska, A. & Jesionowski, T. Zinc Oxide from synthesis to application: A review. *Materials* **7**, 2833-2881; https://doi.org/10.3390/ma7042833 (2014).
6. Zanet, V. *et al.* Activity evaluation of pure and doped zinc oxide nanoparticles against *Saccharomyces cerevisiae*. *J. Appl. Microbiol.***127**, 1391-1402; https://doi.org/10.1111/jam.14407 (2019).
7. Hoseinzadeh, E., Alikhani, M., Samarghandi, M. & Shirzad-Siboni M. Antimicrobial potential of synthesized zinc oxide nanoparticles against gram positive and gram negative bacteria. *Desalination Water Treat.***52**, 4969-4976; https://doi.org/10.1080/19443994.2013.810356 (2014).

8. Jiang, J., Pi, J. & Cai, J. The Advancing of Zinc Oxide Nanoparticles for Biomedical Applications. *Bioinorg. Chem. Appl.* **2018**; https://doi.org/10.1155/2018/1062562 (2018).
9. Tiwari, V., Mishra, N., Gadani, K., Solanki, P.S., Shah, N.A. & Tiwari, M. Mechanism of Anti-bacterial Activity of Zinc Oxide Nanoparticle Against Carbapenem-Resistant *Acinetobacter baumannii*. *Front. Microbiol.***9**, 1218; https://doi.org/10.3389/fmicb.2018.01218 (2018).
10. Alothman, A. A., Albaqami, M. D. Nano sized Cu (II) and Zn (II) complexes and their use as a precursor for synthesis of CuO and ZnO nanoparticles: A study on their sonochemical synthesis, characterization, and DNA/binding/cleavage, anticancer, and antimicrobial activities. *Appl. Organometal. Chem*. **34**, 5827; https://doi.org/10.1002/aoc.5827 (2020).
11. Karekar, S. E. *et al*. Synthesis of zinc molybdate and zinc phosphomolybdate nanopigments by an ultrasound assisted route: Advantage over conventional method. *Chem. Eng*. **87**, 51-59; https://doi.org/10.1016/j.cep.2014.11.010 (2015).
12. Siddiqi, K.S., Rahman, A. & Husen A. Properties of Zinc Oxide Nanoparticles and Their Activity Against Microbes. *Nanoscale Res. Lett.***13**, 141; https://doi.org/10.1186/s11671-018-2532-3 (2018).
13. Agarwal, H., Menon, S., Kumar, S.V. & Rajeshkumar, S. Mechanistic study of the antibacterial action of zinc oxide nanoparticles synthesized using green route. *Chemico-Biol. Inter*. **286**, 60-70; https://doi.org/10.1016/j.cbi.2018.03.008 (2018).
14. Burman, U., Saini, M. & Kumar, P. Effect of zinc oxide nanoparticles on growth and antioxidant system of chickpea seedlings. *Toxicol. Environ. Chem.***95**, 605-612; https://doi.org/10.1080/02772248.2013.803796 (2013).
15. Han, H. *et al.* Recent progress of bacterial FtsZ inhibitors with a focus on peptides. *The FEBS Journal***288**, 1091-1106; https://doi.org/10.1111/febs.15489 (2021).
16. Tripathy, S. & Sahu, S.K. FtsZ inhibitors as a new genera of antibacterial agents. *Bioorg. Chem.***91**, 103-169; https://doi.org/10.1016/j.bioorg.2019.103169 (2019).
17. Król, E. *et al.* Antibacterial activity of alkyl gallates is a combination of direct targeting of FtsZ and permeabilization of bacterial membranes. *Front. Microbiol.***6**, 390; https://doi.org/10.3389/fmicb.2015.00390 (2015).
18. Molnár, Á. *et al.* ZnO nanoparticles induce cell wall remodeling and modify ROS/RNS signalling in roots of Brassica seedlings. *Ecotoxicol. Environ. Saf.***206**, 111-158; https://doi.org/10.1016/j.ecoenv.2020.111158 (2020).
19. Mendes, C. R., Dilarri, G., Stradioto, M.R., Lopes, P. R. M., Bidoia, E. D. & Montagnolli, R. N. Zeta Potential Mechanisms Applied to Cellular Immobilization: A Study with *Saccharomyces cerevisiae* on Dye Adsorption. *J. Polym. Environ*. **29**, 2214-2226; https://doi.org/10.1007/s10924-020-02030-0 (2021).
20. Balouiri, M., Sadiki, M. & Ibnsouda, S.K. Methods for in vitro evaluating antimicrobial activity: a review. *J. Pharm. Anal* **6**, 71-79; https://doi.org/10.1016/j.jpha.2015.11.005 (2016).
21. Vijayakumara, S., Mahadevana, P., Arulmozhia, S., Sriramb, P. K. Green synthesis of zinc oxide nanoparticles using Atalantia monophylla leaf extracts: Characterization and antimicrobial analysis. *Materials Science in Semiconductor Processing***82**, 39-45; https://doi.org/10.1016/j.mssp.2018.03.017 (2018).
22. Subbiah, R., Muthukumaran, S., Raja, V. Biosynthesis, structural, photoluminescence and photocatalytic performance of Mn/Mg dual doped ZnO nanostructures using Ocimum tenuiforum leaf extract. *Optik***208**, 156-166; https://doi.org/10.1016/j.ijleo .2020.164556 (2020).
23. Sheik, M. S., Raj, K. R., Kottaisamy, M., Vasantha, V. S. Biosynthesis of ZnO nanoparticles through extract from Prosopis julifora plant leaf: antibacterial activities and a new approach by rust-induced photocatalysis. *J. Saudi Chem. Soc.***24**, 393-406; https://doi.org/10.1016/j.jscs.2020.03.003 (2020).
24. Khataee, A., Karimi, A., Zarei, M., Joo, S. W. Eu-doped ZnO nanoparticles: sonochemical synthesis, characterization, and sonocatalytic application. *Ultrason Sonochem*. **24**, 393-406; https://doi:10.1016/j.ultsonch.2015.03.016 (2015).
25. Sirelkhatim, A. *et al.* Review on zinc oxide nanoparticles: antibacterial activity and toxicity mechanism. *Nano-Micro Lett*. **7**, 219-242; https://doi.org/10.1007/s40820-015-0040-x (2015).

26. Lundstedt, E., Kahne, D. & Ruiz, N. Assembly and maintenance of lipids at the bacterial outer membrane. *Chemical Reviews***121**, 5098-5123; https://doi.org/10.1021/acs.chemrev.0c00587 (2020).
27. Anitha, R. *et al.* Cytotoxicity, antibacterial and antifungal activities of ZnO nanoparticles prepared by the Artocarpus gomezianus fruit mediated facile green combustion method. *J. Sci. Adv. Mater. Devices***3**, 440-451; https://doi.org/10.1016/j.jsamd.2018.11.001 (2018).
28. Yusof, N. A. A., Zain, N. M. & Pauzi, N. Synthesis of ZnO nanoparticles with chitosan as stabilizing agent and their antibacterial properties against Gram-positive and Gram-negative bacteria. *Int. J. Biol. Macromol*. **124**, 1132-1136; https://doi.org/10.1016/j.ijbiomac.2018.11.228 (2019).
29. Saqib, S. *et al.* Synthesis, characterization and use of iron oxide nano particles for antibacterial activity. *Microscopy Research and Technique***84**, 415-420; https://doi.org/10.1002/jemt.23182 (2019).
30. Zubair, N. & Akhtar, K. Morphology controlled synthesis of ZnO nanoparticles for in-vitro evaluation of antibacterial activity. *Transactions of Nonferrous Metals Society of China***30**, 1605-1614; https://doi.org/10.1016/S1003-6326(20)65323-7 (2020).
31. Du, S., Pichoff, S. & Lutkenhaus, J. FtsEX acts on FtsA to regulate divisome assembly and activity. *Proc. Natl. Acad. Sci.***113**, 52-61; https://doi.org/10.1073/pnas.1606656113 (2016).
32. Hurley, K. A., Santos, T. M., Nepomuceno, G. M., Huynh, V., Shaw, J. T., & Weibel, D. B. Targeting the bacterial division protein ftsz. *J. of Medicinal Chemistry***59**, 6975-6998; https://doi.org/10.1021/acs.jmedchem.5b01098 (2016).
33. Xiao, J., & Goley, E. D. Redefining the roles of the ftsz-ring in bacterial cytokinesis. *Current Opinion in Microbiology***34**, 90-96; https://doi.org/10.1016/j.mib.2016.08.008 (2016).
34. Dilarri, G., Caccalano, M. N., Zamuner, C. F. C., Domingues, D. S., Ferreira, H. Hexanoic acid: a new potential substitute for copper-based agrochemicals against citrus canker. *Journal of Applied Microbiology***131**, 2488-2499; http://dx.doi.org/10.1111/jam.15125 (2021).
35. Abebe, B., Zereffa, E. A., Tadesse, A. & Murthy, H. C. A. A Review on Enhancing the Antibacteril Activity of ZnO: Mechanisms and Microscopic Investigation. *Nanoscale Res. Lett*. **15**, 190; https://doi.org/10.1186/s11671-020-03418-6 (2020).
36. Naqvi, Q. U. A. *et al.* Size-dependent inhibition of bacterial growth by chemically engineered spherical ZnO nanoparticles. *J. Biol. Phys.***45**, 147-159; https://doi.org/10.1016/j.ijbiomac.2018.11.228 (2019).
37. Raj, N. B. *et al.* Harnessing ZnO nanoparticles for antimicrobial and photocatalytic activities. *J. Photochem. Photobiol*. **6**, 100021; https://doi.org/10.1016/j.jpap.2021.100021 (2021).

Figures

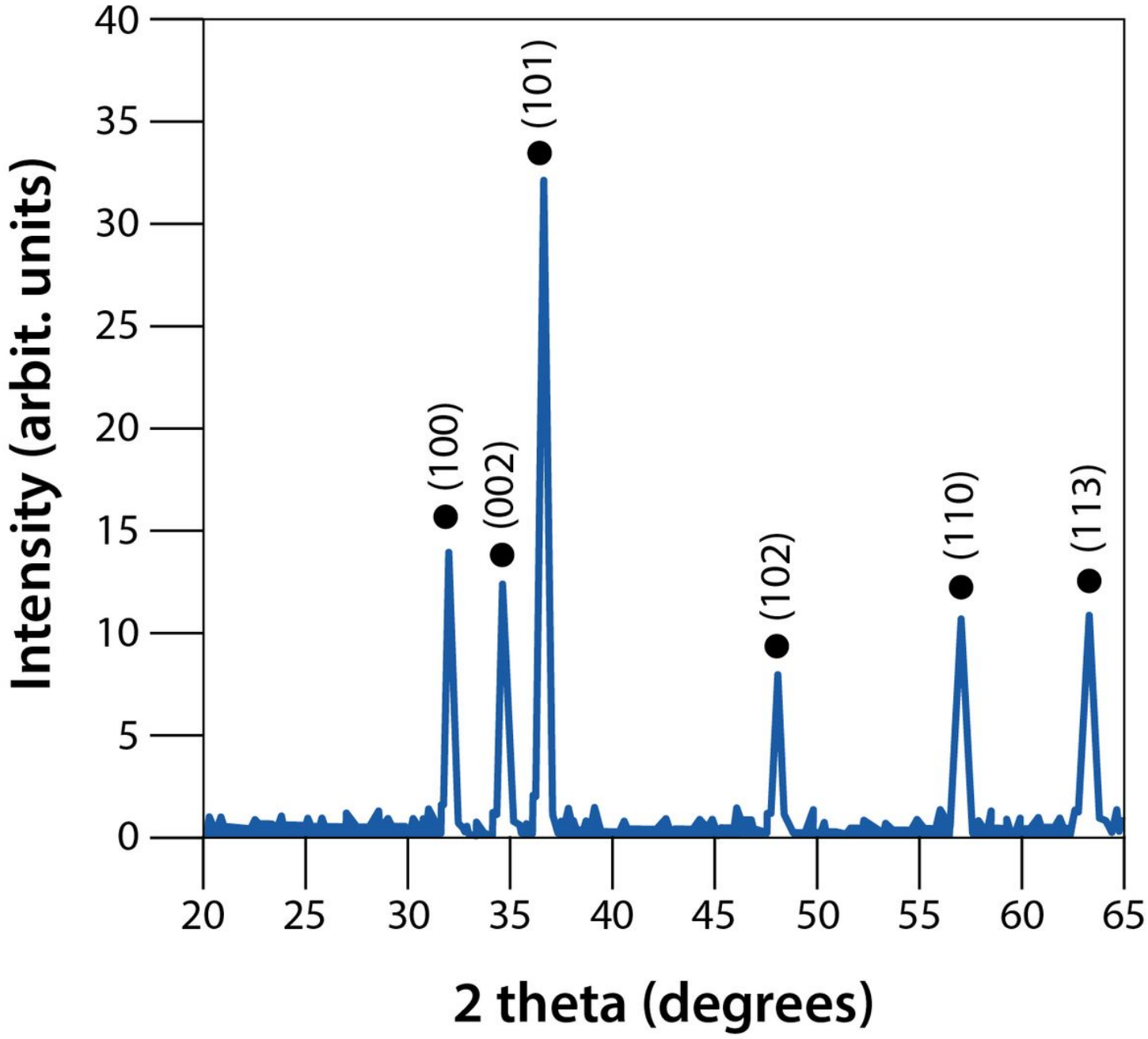

Figure 1

XRD power of ZnO NPs

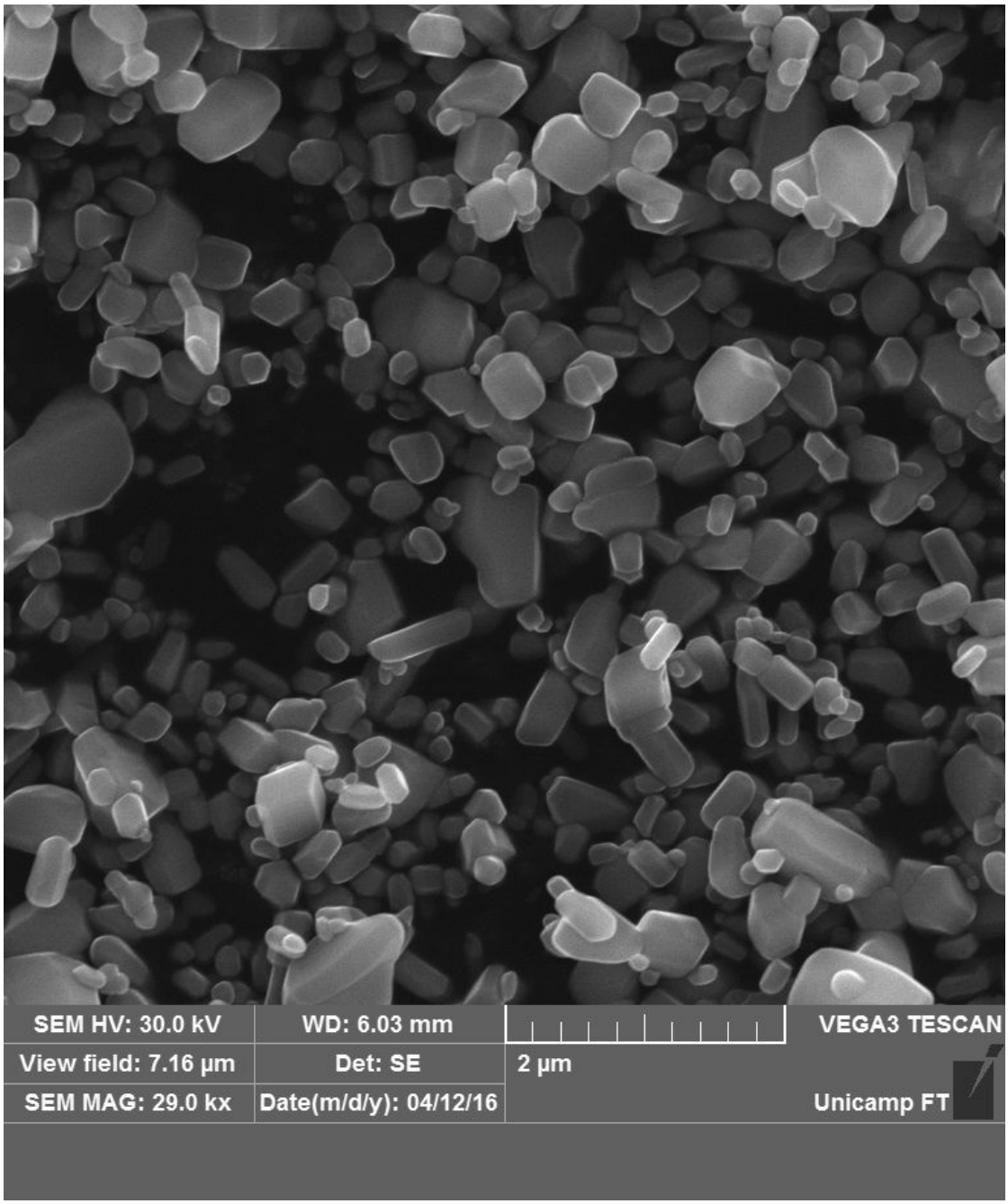

Figure 2

Surface morphology of ZnO NPs by SEM. 2 µm scale bar; 29.0 kx magnification.

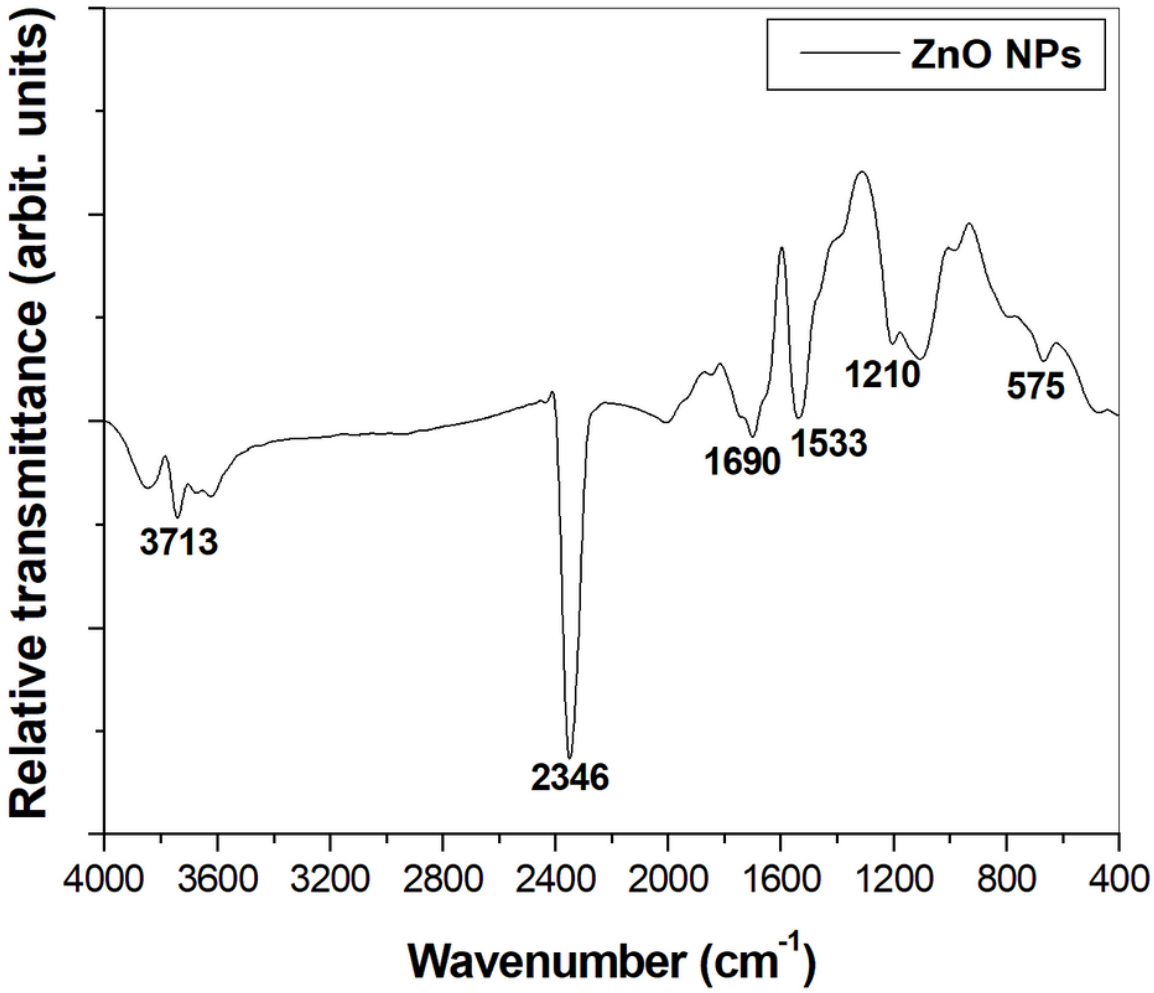

Figure 3

FT-IR spectrum of ZnO NPs.

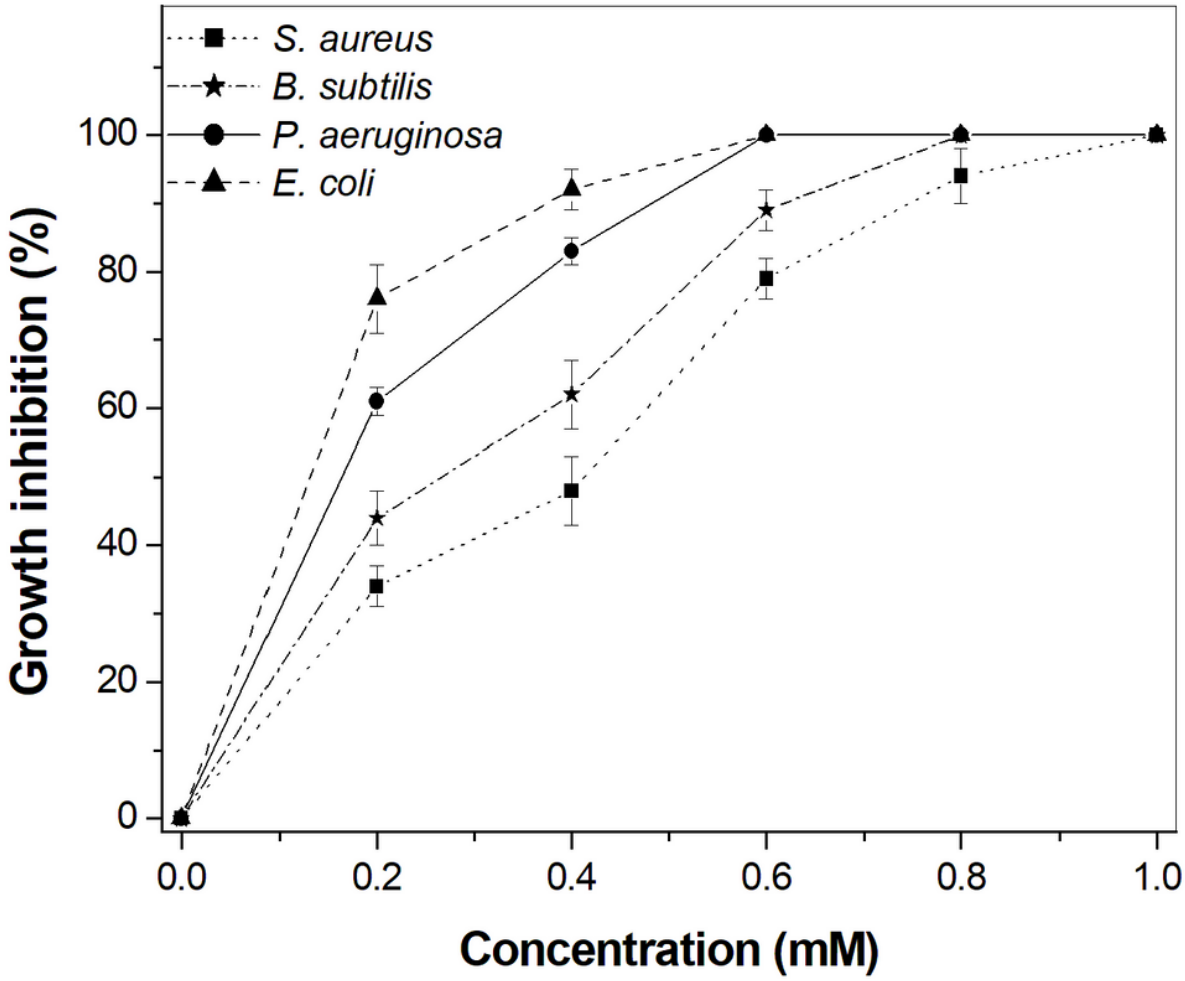

Figure 4

Antimicrobial activity of ZnO NPs determined by REMA from microdilutions with 105 cells in 100 µL.

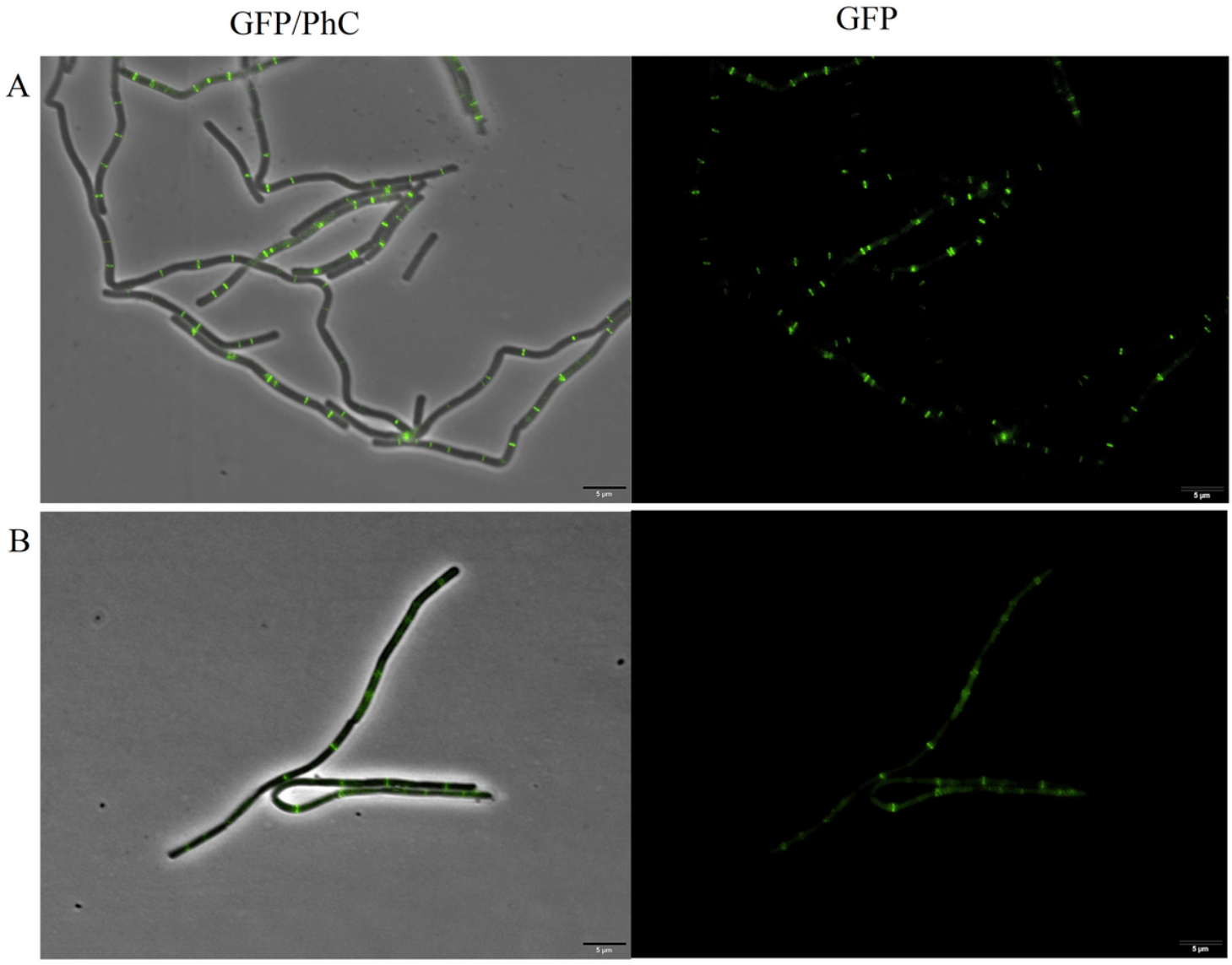

Figure 5

B. subtilis expressing FtsZ-GFP . (A) Control of cells grown in nutrient medium and diluted to 106 cells per mL-1; (B) Cells after 15 min of exposure to ZnO NPs in the IC100. GFP/PhC is the phase contrast images superimposed on the GFP fluorescence images. Scale bar 5 µm; 100× magnification.

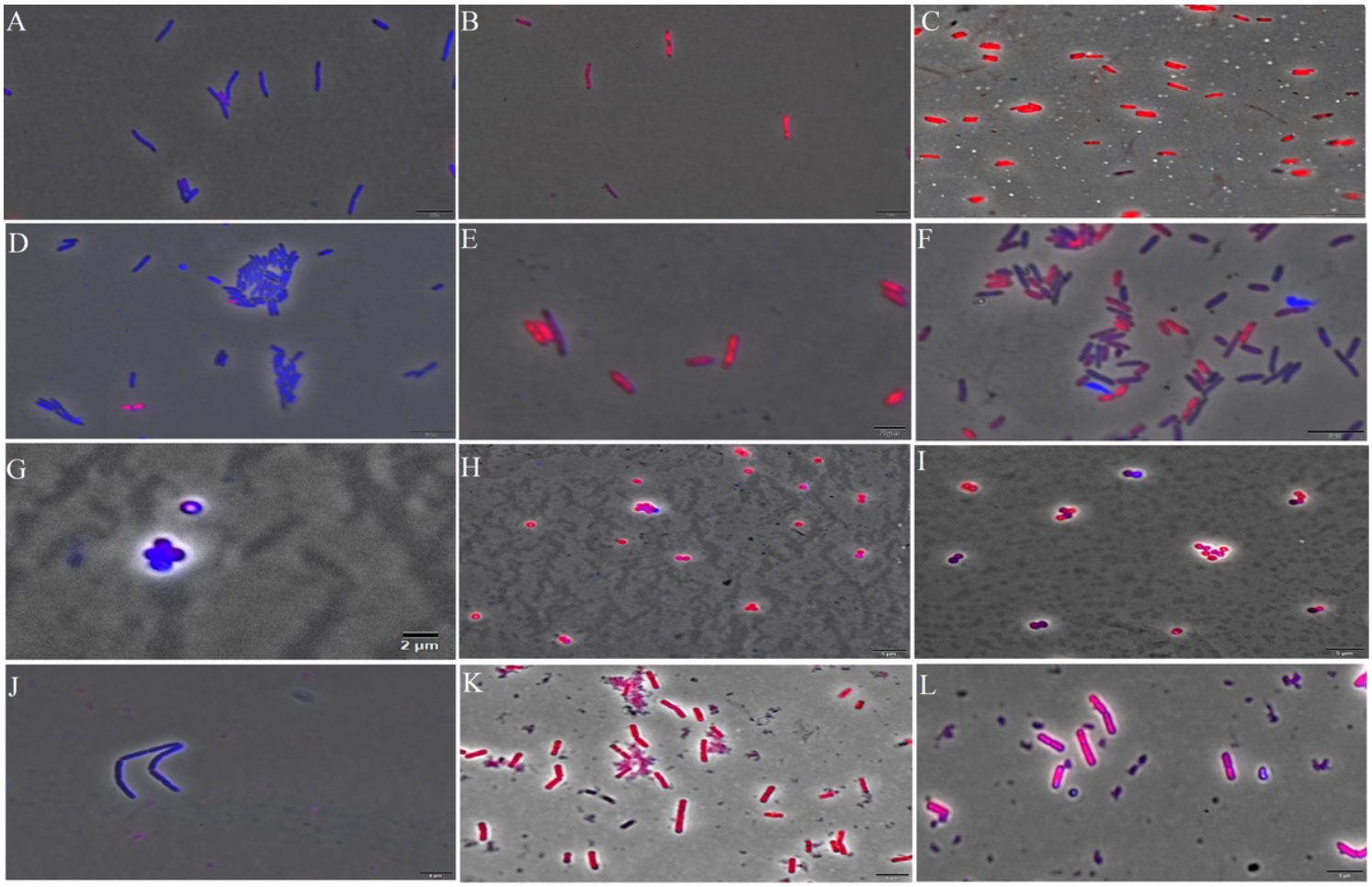

Figure 6

Fluorescence microscopy in cells stained with DAPI and PI after 15 min of exposure to ZnO NPs. Cells with intact membranes are artificially stained in blue, while cells with damaged membranes are stained in red. (A) E. coli (ATCC 8739) cells in nutrient broth medium (negative control); (B) E. coli (ATCC 8739) cells treated with heat-shock stress (positive control); (C) E. coli (ATCC 8739) cells treated with ZnO NPs at IC100; (D) P. aeruginosa (ATCC 27853) cells in nutrient broth medium (negative control); (E) P. aeruginosa (ATCC 27853) cells treated with heat-shock stress (positive control) (F) P. aeruginosa (ATCC 27853) cells treated with ZnO at IC100; (G) S. aureus (ATCC 6538) cells in nutrient broth medium (negative control); (H) S. aureus (ATCC 6538) cells treated with nisin at 5 µg.mL-1 (positive control) (I) S. aureus (ATCC 6538) cells treated with ZnO at IC100; (J) B. subtilis (ATCC 19659) cells in nutrient broth medium (negative control); (K) B. subtilis (ATCC 19659) cells treated with nisin at 5 µg.mL-1 (positive control) (L) B. subtilis (ATCC 19659) cells treated with ZnO at IC100. Scale bar 2 µm; 100× magnification.

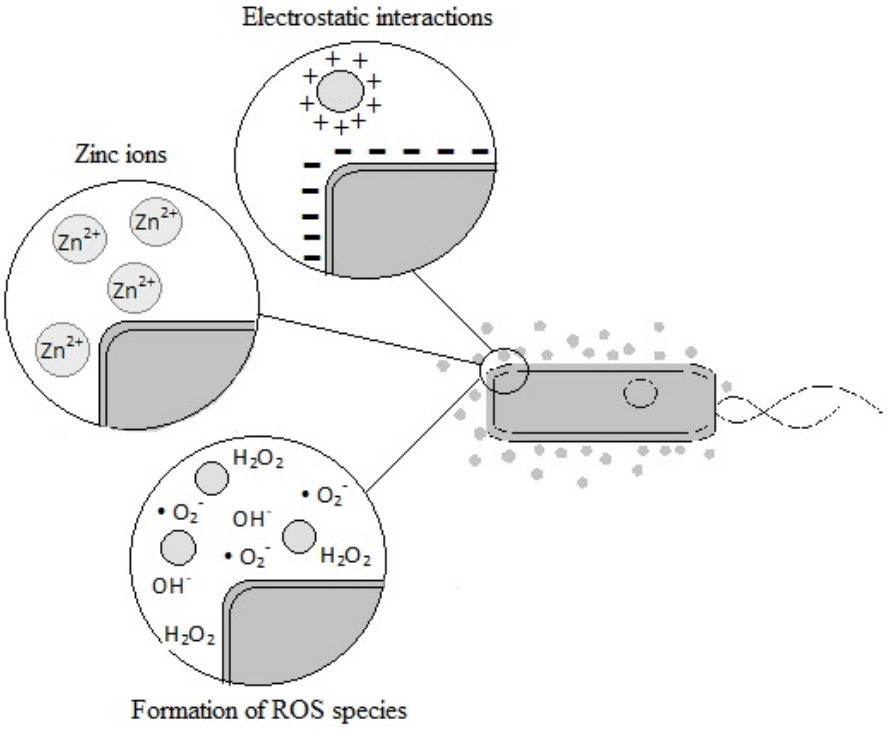

Figure 7

Model of the main bactericidal MOA of ZnO NPs which target the cytoplasmatic membrane and cell wall.

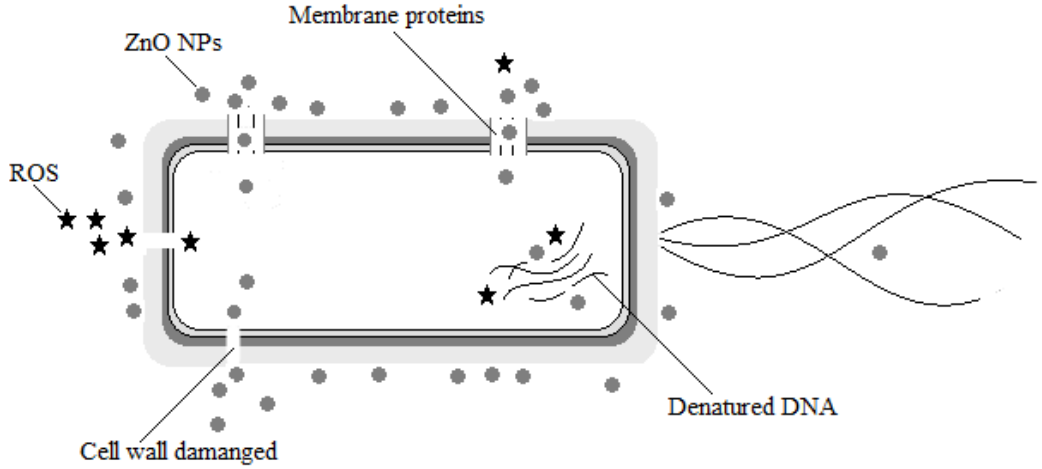

Figure 8

Cell model for the main mechanism of bactericidal action of ZnO NPs.